

# Constraints on spin and parity of the Higgs boson in $VH \rightarrow Vb\bar{b}$ final states

V.M. Abazov,<sup>31</sup> B. Abbott,<sup>67</sup> B.S. Acharya,<sup>25</sup> M. Adams,<sup>46</sup> T. Adams,<sup>44</sup> J.P. Agnew,<sup>41</sup> G.D. Alexeev,<sup>31</sup> G. Alkhazov,<sup>35</sup> A. Alton<sup>a,56</sup> A. Askew,<sup>44</sup> S. Atkins,<sup>54</sup> K. Augsten,<sup>7</sup> C. Avila,<sup>5</sup> F. Badaud,<sup>10</sup> L. Bagby,<sup>45</sup> B. Baldin,<sup>45</sup> D.V. Bandurin,<sup>73</sup> S. Banerjee,<sup>25</sup> E. Barberis,<sup>55</sup> P. Baringer,<sup>53</sup> J.F. Bartlett,<sup>45</sup> U. Bassler,<sup>15</sup> V. Bazterra,<sup>46</sup> A. Bean,<sup>53</sup> M. Begalli,<sup>2</sup> L. Bellantoni,<sup>45</sup> S.B. Beri,<sup>23</sup> G. Bernardi,<sup>14</sup> R. Bernhard,<sup>19</sup> I. Bertram,<sup>39</sup> M. Besançon,<sup>15</sup> R. Beuselinck,<sup>40</sup> P.C. Bhat,<sup>45</sup> S. Bhatia,<sup>58</sup> V. Bhatnagar,<sup>23</sup> G. Blazey,<sup>47</sup> S. Blessing,<sup>44</sup> K. Bloom,<sup>59</sup> A. Boehnlein,<sup>45</sup> D. Boline,<sup>64</sup> E.E. Boos,<sup>33</sup> G. Borissov,<sup>39</sup> M. Borysova<sup>l,38</sup> A. Brandt,<sup>70</sup> O. Brandt,<sup>20</sup> R. Brock,<sup>57</sup> A. Bross,<sup>45</sup> D. Brown,<sup>14</sup> X.B. Bu,<sup>45</sup> M. Buehler,<sup>45</sup> V. Buescher,<sup>21</sup> V. Bunichev,<sup>33</sup> S. Burdin<sup>b,39</sup> C.P. Buszello,<sup>37</sup> E. Camacho-Pérez,<sup>28</sup> B.C.K. Casey,<sup>45</sup> H. Castilla-Valdez,<sup>28</sup> S. Caughron,<sup>57</sup> S. Chakrabarti,<sup>64</sup> K.M. Chan,<sup>51</sup> A. Chandra,<sup>72</sup> E. Chapon,<sup>15</sup> G. Chen,<sup>53</sup> S.W. Cho,<sup>27</sup> S. Choi,<sup>27</sup> B. Choudhary,<sup>24</sup> S. Cihangir,<sup>45</sup> D. Claes,<sup>59</sup> J. Clutter,<sup>53</sup> M. Cooke<sup>k,45</sup> W.E. Cooper,<sup>45</sup> M. Corcoran,<sup>72</sup> F. Couderc,<sup>15</sup> M.-C. Cousinou,<sup>12</sup> D. Cutts,<sup>69</sup> A. Das,<sup>42</sup> G. Davies,<sup>40</sup> S.J. de Jong,<sup>29,30</sup> E. De La Cruz-Burelo,<sup>28</sup> F. Déliot,<sup>15</sup> R. Demina,<sup>63</sup> D. Denisov,<sup>45</sup> S.P. Denisov,<sup>34</sup> S. Desai,<sup>45</sup> C. Deterre<sup>c,20</sup> K. DeVaughan,<sup>59</sup> H.T. Diehl,<sup>45</sup> M. Diesburg,<sup>45</sup> P.F. Ding,<sup>41</sup> A. Dominguez,<sup>59</sup> A. Dubey,<sup>24</sup> L.V. Dudko,<sup>33</sup> A. Duperrin,<sup>12</sup> S. Dutt,<sup>23</sup> M. Eads,<sup>47</sup> D. Edmunds,<sup>57</sup> J. Ellison,<sup>43</sup> V.D. Elvira,<sup>45</sup> Y. Enari,<sup>14</sup> H. Evans,<sup>49</sup> V.N. Evdokimov,<sup>34</sup> A. Fauré,<sup>15</sup> L. Feng,<sup>47</sup> T. Ferbel,<sup>63</sup> F. Fiedler,<sup>21</sup> F. Filthaut,<sup>29,30</sup> W. Fisher,<sup>57</sup> H.E. Fisk,<sup>45</sup> M. Fortner,<sup>47</sup> H. Fox,<sup>39</sup> S. Fuess,<sup>45</sup> P.H. Garbincius,<sup>45</sup> A. Garcia-Bellido,<sup>63</sup> J.A. García-González,<sup>28</sup> V. Gavrilov,<sup>32</sup> W. Geng,<sup>12,57</sup> C.E. Gerber,<sup>46</sup> Y. Gershtein,<sup>60</sup> G. Ginther,<sup>45,63</sup> O. Gogota,<sup>38</sup> G. Golovanov,<sup>31</sup> P.D. Grannis,<sup>64</sup> S. Greder,<sup>16</sup> H. Greenlee,<sup>45</sup> G. Grenier,<sup>17</sup> Ph. Gris,<sup>10</sup> J.-F. Grivaz,<sup>13</sup> A. Grohsjean<sup>c,15</sup> S. Grünendahl,<sup>45</sup> M.W. Grünewald,<sup>26</sup> T. Guillemin,<sup>13</sup> G. Gutierrez,<sup>45</sup> P. Gutierrez,<sup>67</sup> J. Haley,<sup>68</sup> L. Han,<sup>4</sup> K. Harder,<sup>41</sup> A. Harel,<sup>63</sup> J.M. Hauptman,<sup>52</sup> J. Hays,<sup>40</sup> T. Head,<sup>41</sup> T. Hebbeker,<sup>18</sup> D. Hedin,<sup>47</sup> H. Hegab,<sup>68</sup> A.P. Heinson,<sup>43</sup> U. Heintz,<sup>69</sup> C. Hensel,<sup>1</sup> I. Heredia-De La Cruz<sup>d,28</sup> K. Herner,<sup>45</sup> G. Hesketh<sup>f,41</sup> M.D. Hildreth,<sup>51</sup> R. Hirosky,<sup>73</sup> T. Hoang,<sup>44</sup> J.D. Hobbs,<sup>64</sup> B. Hoeneisen,<sup>9</sup> J. Hogan,<sup>72</sup> M. Hohlfeld,<sup>21</sup> J.L. Holzbauer,<sup>58</sup> I. Howley,<sup>70</sup> Z. Hubacek,<sup>7,15</sup> V. Hynek,<sup>7</sup> I. Iashvili,<sup>62</sup> Y. Ilchenko,<sup>71</sup> R. Illingworth,<sup>45</sup> A.S. Ito,<sup>45</sup> S. Jabeen<sup>m,45</sup> M. Jaffré,<sup>13</sup> A. Jayasinghe,<sup>67</sup> M.S. Jeong,<sup>27</sup> R. Jesik,<sup>40</sup> P. Jiang,<sup>4</sup> K. Johns,<sup>42</sup> E. Johnson,<sup>57</sup> M. Johnson,<sup>45</sup> A. Jonckheere,<sup>45</sup> P. Jonsson,<sup>40</sup> J. Joshi,<sup>43</sup> A.W. Jung,<sup>45</sup> A. Juste,<sup>36</sup> E. Kajfasz,<sup>12</sup> D. Karmanov,<sup>33</sup> I. Katsanos,<sup>59</sup> R. Kehoe,<sup>71</sup> S. Kermiche,<sup>12</sup> N. Khalatyan,<sup>45</sup> A. Khanov,<sup>68</sup> A. Kharchilava,<sup>62</sup> Y.N. Kharzheev,<sup>31</sup> I. Kiselevich,<sup>32</sup> J.M. Kohli,<sup>23</sup> A.V. Kozelov,<sup>34</sup> J. Kraus,<sup>58</sup> A. Kumar,<sup>62</sup> A. Kupco,<sup>8</sup> T. Kurča,<sup>17</sup> V.A. Kuzmin,<sup>33</sup> S. Lammers,<sup>49</sup> P. Lebrun,<sup>17</sup> H.S. Lee,<sup>27</sup> S.W. Lee,<sup>52</sup> W.M. Lee,<sup>45</sup> X. Lei,<sup>42</sup> J. Lellouch,<sup>14</sup> D. Li,<sup>14</sup> H. Li,<sup>73</sup> L. Li,<sup>43</sup> Q.Z. Li,<sup>45</sup> J.K. Lim,<sup>27</sup> D. Lincoln,<sup>45</sup> J. Linnemann,<sup>57</sup> V.V. Lipaev,<sup>34</sup> R. Lipton,<sup>45</sup> H. Liu,<sup>71</sup> Y. Liu,<sup>4</sup> A. Lobodenko,<sup>35</sup> M. Lokajicek,<sup>8</sup> R. Lopes de Sa,<sup>64</sup> R. Luna-Garcia<sup>g,28</sup> A.L. Lyon,<sup>45</sup> A.K.A. Maciel,<sup>1</sup> R. Madar,<sup>19</sup> R. Magaña-Villalba,<sup>28</sup> S. Malik,<sup>59</sup> V.L. Malyshev,<sup>31</sup> J. Mansour,<sup>20</sup> J. Martínez-Ortega,<sup>28</sup> R. McCarthy,<sup>64</sup> C.L. McGivern,<sup>41</sup> M.M. Meijer,<sup>29,30</sup> A. Melnitchouk,<sup>45</sup> D. Menezes,<sup>47</sup> P.G. Mercadante,<sup>3</sup> M. Merkin,<sup>33</sup> A. Meyer,<sup>18</sup> J. Meyer<sup>i,20</sup> F. Miconi,<sup>16</sup> N.K. Mondal,<sup>25</sup> M. Mulhearn,<sup>73</sup> E. Nagy,<sup>12</sup> M. Narain,<sup>69</sup> R. Nayyar,<sup>42</sup> H.A. Neal,<sup>56</sup> J.P. Negret,<sup>5</sup> P. Neustroev,<sup>35</sup> H.T. Nguyen,<sup>73</sup> T. Nunnemann,<sup>22</sup> J. Orduna,<sup>72</sup> N. Osman,<sup>12</sup> J. Osta,<sup>51</sup> A. Pal,<sup>70</sup> N. Parashar,<sup>50</sup> V. Parihar,<sup>69</sup> S.K. Park,<sup>27</sup> R. Partridge<sup>e,69</sup> N. Parua,<sup>49</sup> A. Patwa<sup>j,65</sup> B. Penning,<sup>45</sup> M. Perfilov,<sup>33</sup> Y. Peters,<sup>41</sup> K. Petridis,<sup>41</sup> G. Petrillo,<sup>63</sup> P. Pétroff,<sup>13</sup> M.-A. Pleier,<sup>65</sup> V.M. Podstavkov,<sup>45</sup> A.V. Popov,<sup>34</sup> M. Prewitt,<sup>72</sup> D. Price,<sup>41</sup> N. Prokopenko,<sup>34</sup> J. Qian,<sup>56</sup> A. Quadt,<sup>20</sup> B. Quinn,<sup>58</sup> P.N. Ratoff,<sup>39</sup> I. Razumov,<sup>34</sup> I. Ripp-Baudot,<sup>16</sup> F. Rizatdinova,<sup>68</sup> M. Rominsky,<sup>45</sup> A. Ross,<sup>39</sup> C. Royon,<sup>15</sup> P. Rubinov,<sup>45</sup> R. Ruchti,<sup>51</sup> G. Sajot,<sup>11</sup> A. Sánchez-Hernández,<sup>28</sup> M.P. Sanders,<sup>22</sup> A.S. Santos<sup>h,1</sup> G. Savage,<sup>45</sup> M. Savitskyi,<sup>38</sup> L. Sawyer,<sup>54</sup> T. Scanlon,<sup>40</sup> R.D. Schamberger,<sup>64</sup> Y. Scheglov,<sup>35</sup> H. Schellman,<sup>48</sup> C. Schwanenberger,<sup>41</sup> R. Schwienhorst,<sup>57</sup> J. Sekaric,<sup>53</sup> H. Severini,<sup>67</sup> E. Shabalina,<sup>20</sup> V. Shary,<sup>15</sup> S. Shaw,<sup>57</sup> A.A. Shchukin,<sup>34</sup> V. Simak,<sup>7</sup> P. Skubic,<sup>67</sup> P. Slatery,<sup>63</sup> D. Smirnov,<sup>51</sup> G.R. Snow,<sup>59</sup> J. Snow,<sup>66</sup> S. Snyder,<sup>65</sup> S. Söldner-Rembold,<sup>41</sup> L. Sonnenschein,<sup>18</sup> K. Soustruznik,<sup>6</sup> J. Stark,<sup>11</sup> D.A. Stoyanova,<sup>34</sup> M. Strauss,<sup>67</sup> L. Suter,<sup>41</sup> P. Svoisky,<sup>67</sup> M. Titov,<sup>15</sup> V.V. Tokmenin,<sup>31</sup> Y.-T. Tsai,<sup>63</sup> D. Tsybychev,<sup>64</sup> B. Tuchming,<sup>15</sup> C. Tully,<sup>61</sup> L. Uvarov,<sup>35</sup> S. Uvarov,<sup>35</sup> S. Uzunyan,<sup>47</sup> R. Van Kooten,<sup>49</sup> W.M. van Leeuwen,<sup>29</sup> N. Varelas,<sup>46</sup> E.W. Varnes,<sup>42</sup> I.A. Vasilyev,<sup>34</sup> A.Y. Verkheev,<sup>31</sup> L.S. Vertogradov,<sup>31</sup> M. Verzocchi,<sup>45</sup> M. Vesterinen,<sup>41</sup> D. Vilanova,<sup>15</sup> P. Vokac,<sup>7</sup> H.D. Wahl,<sup>44</sup> M.H.L.S. Wang,<sup>45</sup> J. Warchol,<sup>51</sup> G. Watts,<sup>74</sup> M. Wayne,<sup>51</sup> J. Weichert,<sup>21</sup> L. Welty-Rieger,<sup>48</sup>

M.R.J. Williams,<sup>49</sup> G.W. Wilson,<sup>53</sup> M. Wobisch,<sup>54</sup> D.R. Wood,<sup>55</sup> T.R. Wyatt,<sup>41</sup> Y. Xie,<sup>45</sup> R. Yamada,<sup>45</sup> S. Yang,<sup>4</sup> T. Yasuda,<sup>45</sup> Y.A. Yatsunenko,<sup>31</sup> W. Ye,<sup>64</sup> Z. Ye,<sup>45</sup> H. Yin,<sup>45</sup> K. Yip,<sup>65</sup> S.W. Youn,<sup>45</sup> J.M. Yu,<sup>56</sup> J. Zennamo,<sup>62</sup> T.G. Zhao,<sup>41</sup> B. Zhou,<sup>56</sup> J. Zhu,<sup>56</sup> M. Zielinski,<sup>63</sup> D. Zieminska,<sup>49</sup> and L. Zivkovic<sup>14</sup>

(The D0 Collaboration\*)

<sup>1</sup>LAFEX, Centro Brasileiro de Pesquisas Físicas, Rio de Janeiro, Brazil

<sup>2</sup>Universidade do Estado do Rio de Janeiro, Rio de Janeiro, Brazil

<sup>3</sup>Universidade Federal do ABC, Santo André, Brazil

<sup>4</sup>University of Science and Technology of China, Hefei, People's Republic of China

<sup>5</sup>Universidad de los Andes, Bogotá, Colombia

<sup>6</sup>Charles University, Faculty of Mathematics and Physics,

Center for Particle Physics, Prague, Czech Republic

<sup>7</sup>Czech Technical University in Prague, Prague, Czech Republic

<sup>8</sup>Institute of Physics, Academy of Sciences of the Czech Republic, Prague, Czech Republic

<sup>9</sup>Universidad San Francisco de Quito, Quito, Ecuador

<sup>10</sup>LPC, Université Blaise Pascal, CNRS/IN2P3, Clermont, France

<sup>11</sup>LPSC, Université Joseph Fourier Grenoble 1, CNRS/IN2P3,

Institut National Polytechnique de Grenoble, Grenoble, France

<sup>12</sup>CPPM, Aix-Marseille Université, CNRS/IN2P3, Marseille, France

<sup>13</sup>LAL, Université Paris-Sud, CNRS/IN2P3, Orsay, France

<sup>14</sup>LPNHE, Universités Paris VI and VII, CNRS/IN2P3, Paris, France

<sup>15</sup>CEA, Irfu, SPP, Saclay, France

<sup>16</sup>IPHC, Université de Strasbourg, CNRS/IN2P3, Strasbourg, France

<sup>17</sup>IPNL, Université Lyon 1, CNRS/IN2P3, Villeurbanne, France and Université de Lyon, Lyon, France

<sup>18</sup>III. Physikalisches Institut A, RWTH Aachen University, Aachen, Germany

<sup>19</sup>Physikalisches Institut, Universität Freiburg, Freiburg, Germany

<sup>20</sup>II. Physikalisches Institut, Georg-August-Universität Göttingen, Göttingen, Germany

<sup>21</sup>Institut für Physik, Universität Mainz, Mainz, Germany

<sup>22</sup>Ludwig-Maximilians-Universität München, München, Germany

<sup>23</sup>Panjab University, Chandigarh, India

<sup>24</sup>Delhi University, Delhi, India

<sup>25</sup>Tata Institute of Fundamental Research, Mumbai, India

<sup>26</sup>University College Dublin, Dublin, Ireland

<sup>27</sup>Korea Detector Laboratory, Korea University, Seoul, Korea

<sup>28</sup>CINVESTAV, Mexico City, Mexico

<sup>29</sup>Nikhef, Science Park, Amsterdam, the Netherlands

<sup>30</sup>Radboud University Nijmegen, Nijmegen, the Netherlands

<sup>31</sup>Joint Institute for Nuclear Research, Dubna, Russia

<sup>32</sup>Institute for Theoretical and Experimental Physics, Moscow, Russia

<sup>33</sup>Moscow State University, Moscow, Russia

<sup>34</sup>Institute for High Energy Physics, Protvino, Russia

<sup>35</sup>Petersburg Nuclear Physics Institute, St. Petersburg, Russia

<sup>36</sup>Institució Catalana de Recerca i Estudis Avançats (ICREA) and Institut de Física d'Altes Energies (IFAE), Barcelona, Spain

<sup>37</sup>Uppsala University, Uppsala, Sweden

<sup>38</sup>Taras Shevchenko National University of Kyiv, Kiev, Ukraine

<sup>39</sup>Lancaster University, Lancaster LA1 4YB, United Kingdom

<sup>40</sup>Imperial College London, London SW7 2AZ, United Kingdom

<sup>41</sup>The University of Manchester, Manchester M13 9PL, United Kingdom

<sup>42</sup>University of Arizona, Tucson, Arizona 85721, USA

<sup>43</sup>University of California Riverside, Riverside, California 92521, USA

<sup>44</sup>Florida State University, Tallahassee, Florida 32306, USA

<sup>45</sup>Fermi National Accelerator Laboratory, Batavia, Illinois 60510, USA

<sup>46</sup>University of Illinois at Chicago, Chicago, Illinois 60607, USA

<sup>47</sup>Northern Illinois University, DeKalb, Illinois 60115, USA

<sup>48</sup>Northwestern University, Evanston, Illinois 60208, USA

<sup>49</sup>Indiana University, Bloomington, Indiana 47405, USA

<sup>50</sup>Purdue University Calumet, Hammond, Indiana 46323, USA

<sup>51</sup>University of Notre Dame, Notre Dame, Indiana 46556, USA

<sup>52</sup>Iowa State University, Ames, Iowa 50011, USA

<sup>53</sup>University of Kansas, Lawrence, Kansas 66045, USA

<sup>54</sup>Louisiana Tech University, Ruston, Louisiana 71272, USA

<sup>55</sup>Northeastern University, Boston, Massachusetts 02115, USA

<sup>56</sup>University of Michigan, Ann Arbor, Michigan 48109, USA

<sup>57</sup>Michigan State University, East Lansing, Michigan 48824, USA

<sup>58</sup>University of Mississippi, University, Mississippi 38677, USA

<sup>59</sup>University of Nebraska, Lincoln, Nebraska 68588, USA

<sup>60</sup>Rutgers University, Piscataway, New Jersey 08855, USA

<sup>61</sup>Princeton University, Princeton, New Jersey 08544, USA

<sup>62</sup>State University of New York, Buffalo, New York 14260, USA

<sup>63</sup>University of Rochester, Rochester, New York 14627, USA

<sup>64</sup>State University of New York, Stony Brook, New York 11794, USA

<sup>65</sup>Brookhaven National Laboratory, Upton, New York 11973, USA

<sup>66</sup>Langston University, Langston, Oklahoma 73050, USA

<sup>67</sup>University of Oklahoma, Norman, Oklahoma 73019, USA

<sup>68</sup>Oklahoma State University, Stillwater, Oklahoma 74078, USA

<sup>69</sup>Brown University, Providence, Rhode Island 02912, USA

<sup>70</sup>University of Texas, Arlington, Texas 76019, USA

<sup>71</sup>Southern Methodist University, Dallas, Texas 75275, USA

<sup>72</sup>Rice University, Houston, Texas 77005, USA

<sup>73</sup>University of Virginia, Charlottesville, Virginia 22904, USA

<sup>74</sup>University of Washington, Seattle, Washington 98195, USA

(Dated: July 23, 2014)

We present the first constraints on the spin  $J$  and parity  $P$  of the Higgs boson,  $H$ , decaying to two  $b$  quarks in up to  $9.7 \text{ fb}^{-1}$  of  $p\bar{p}$  collisions at  $\sqrt{s} = 1.96 \text{ TeV}$  collected with the D0 detector at the Fermilab Tevatron Collider. In the  $ZH \rightarrow \ell\bar{\ell}b\bar{b}$ ,  $WH \rightarrow \ell\nu b\bar{b}$ , and  $ZH \rightarrow \nu\nu b\bar{b}$  final states, we compare the standard model (SM) Higgs boson hypothesis,  $J^P = 0^+$ , with two alternative hypotheses,  $J^P = 0^-$  and  $J^P = 2^+$ . We use a likelihood ratio to quantify the level of preference in data for the  $J^P = 0^+$  prediction. We reject the  $J^P = 0^-$  and  $J^P = 2^+$  hypotheses at the 97.6% CL and at the 99.0% CL, respectively, assuming that the product of the signal production cross section and the branching fraction into  $b\bar{b}$  is equal to the SM prediction. The expected exclusion sensitivity for a  $J^P = 0^-$  ( $J^P = 2^+$ ) state is at the 99.86% (99.94%) CL. For completeness, other production rates are also considered. When considering the hypothesis that our data is the result of a combination of the SM-like Higgs boson and either a  $J^P = 0^-$  or a  $J^P = 2^+$  signal, we exclude a  $J^P = 0^-$  fraction above 0.80 and a  $J^P = 2^+$  fraction above 0.67 at the 95% CL. The expected exclusion covers  $J^P = 0^-$  ( $J^P = 2^+$ ) fractions above 0.54 (0.47).

PACS numbers: 14.80.Bn, 14.80.Ec, 13.85.Rm

After the discovery of a Higgs boson,  $H$ , at the CERN Large Hadron Collider (LHC) [1, 2] in bosonic final states, and evidence for its decay to a pair of  $b$  quarks at the Tevatron experiments [3], it is important to determine the new particle's properties using all decay modes available. In particular, the spin and parity of the Higgs boson are important in determining the framework of the mass generation mechanism. The SM predicts that the Higgs boson is a CP-even spin-0 particle ( $J^P = 0^+$ ). If the Higgs boson is indeed a single boson, the observation

of its decay to two photons at the LHC precludes spin 1 according to the Landau-Yang theorem [4, 5]. Other  $J^P$  possibilities are easily motivated. An admixture of  $J^P = 0^+$  and  $J^P = 0^-$  can arise in Two-Higgs-Doublet models (2HDM) [6, 7] of type II such as found in supersymmetric models. A boson with tensor couplings ( $J^P = 2^+$ ) can arise in models with extra dimensions [8]. The ATLAS and CMS Collaborations have examined the possibility that the  $H$  boson has  $J^P = 0^-$  or  $J^P = 2^+$  using its decays to  $\gamma\gamma$ ,  $ZZ$ , and  $WW$  states [9–11]; however, the  $b\bar{b}$  final state has not yet been studied. The  $J^P = 2^+$  hypothesis is excluded at the 99.9% CL by the ATLAS Collaboration when combining all bosonic decay modes. Likewise, the  $J^P = 0^-$  hypothesis is excluded at the 97.8% and  $\geq 97.7\%$  CL by the ATLAS and CMS Collaborations, respectively, in the  $H \rightarrow ZZ \rightarrow 4\ell$  decay mode. In this Letter we present a study of the Higgs boson spin and parity assignments of  $J^P = 0^-$  or  $J^P = 2^+$  using the  $b\bar{b}$  decay mode. We explore two scenarios for each of the hypotheses: (a) the new boson is a  $J^P = 0^-$  ( $J^P = 2^+$ ) particle and (b) the observed resonance is either a combination of these non-SM  $J^P$  states or distinct states with degenerate mass. In the latter, we do not consider interference effects between states.

\*with visitors from <sup>a</sup>Augustana College, Sioux Falls, SD, USA,

<sup>b</sup>The University of Liverpool, Liverpool, UK, <sup>c</sup>DESY, Hamburg, Germany, <sup>d</sup>Universidad Michoacana de San Nicolas de Hidalgo, Morelia, Mexico <sup>e</sup>SLAC, Menlo Park, CA, USA, <sup>f</sup>University College London, London, UK, <sup>g</sup>Centro de Investigacion en Computacion - IPN, Mexico City, Mexico, <sup>h</sup>Universidade Estadual Paulista, São Paulo, Brazil, <sup>i</sup>Karlsruher Institut für Technologie (KIT) - Steinbuch Centre for Computing (SCC), D-76128 Karlsruhe, Germany, <sup>j</sup>Office of Science, U.S. Department of Energy, Washington, D.C. 20585, USA, <sup>k</sup>American Association for the Advancement of Science, Washington, D.C. 20005, USA, <sup>l</sup>Kiev Institute for Nuclear Research, Kiev, Ukraine and <sup>m</sup>University of Maryland, College Park, Maryland 20742, USA.

Unlike the LHC  $J^P$  measurements, our ability to distinguish different Higgs boson  $J^P$  assignments is not based primarily on the angular analysis of the Higgs boson decay products. It is instead based on the kinematic correlations between the vector boson  $V(V = W, Z)$  and the Higgs boson in  $VH$  associated production. Searches for associated  $VH$  production are sensitive to the different kinematics of the various  $J^P$  combinations in several observables, especially in the invariant mass of the  $VH$  system, due to the dominant  $p$  and  $d$  wave contributions to the  $J^P = 0^-$  and  $J^P = 2^+$  production processes [12–14]. The dominant  $p$  and  $d$  wave contributions to the production cross sections near threshold vary as  $\beta^3$  and  $\beta^5$ , respectively, whereas the dominant  $s$  wave contribution for the SM Higgs boson varies as  $\beta$ . Here,  $\beta = p_H/E_H$  is given by the ratio of the Higgs boson’s momentum and energy.

To probe the Higgs boson spin and parity we use the D0 studies of  $ZH \rightarrow \ell\ell b\bar{b}$  [15],  $WH \rightarrow \ell\nu b\bar{b}$  [16], and  $ZH \rightarrow \nu\nu b\bar{b}$  [17] with no modifications to the event selections. Lepton flavors considered in the  $WH \rightarrow \ell\nu b\bar{b}$  and  $ZH \rightarrow \ell\ell b\bar{b}$  analyses include electrons and muons. Events with taus that decay to these leptons are considered as well, although their contribution is small. The D0 detector, described in detail in Refs. [18–20], consists of a silicon microstrip tracker and a central fiber tracker inside a 1.9 T solenoid, a liquid argon and uranium calorimeter, and an outer muon system consisting of layers of tracking detectors and scintillation counters that surrounds a 1.8 T iron toroid.

We use 9.5–9.7 fb $^{-1}$  of integrated luminosity collected with the D0 detector satisfying relevant data-quality requirements in each of the three analyses. The SM background processes are either estimated from dedicated data samples (multijet backgrounds), or from Monte Carlo (MC) simulation. The  $V$ +jets and  $t\bar{t}$  processes are generated using ALPGEN [21], single top processes are generated using SINGLETOP [22], and diboson ( $VV$ ) processes are generated using PYTHIA [23]. The SM Higgs boson processes are also generated using PYTHIA. The signal samples for the  $J^P = 0^-$  and  $J^P = 2^+$  hypotheses are generated using MADGRAPH 5 [24]. As a cross check of the MADGRAPH simulation, we have verified that  $J^P = 0^+$  samples produced with MADGRAPH agree well with the SM PYTHIA prediction.

In the following, we denote a non-SM Higgs boson as  $X$ , reserving the label  $H$  for the SM  $J^P = 0^+$  Higgs boson. MADGRAPH can simulate several non-SM models, as well as user-defined models. These new states are introduced via dimension-5 Lagrangian operators [13]. The  $J^P = 0^-$  samples are created using a model from the authors of Ref. [12]. The non-SM Lagrangian can be expressed as [13]  $\mathcal{L}_{0^-} = \frac{c_V^A}{\Lambda} A F_{\mu\nu} \tilde{F}^{\mu\nu}$ , where  $F_{\mu\nu}$  is the field-strength tensor for the vector boson,  $\tilde{F}^{\mu\nu}$  is the dual field-strength tensor,  $A$  is the new boson field,  $c_V^A$  is a

coupling term, and  $\Lambda$  is the scale at which new physics effects arise. The  $J^P = 2^+$  signal samples are created using a Randall-Sundrum (RS) model, an extra-dimension model with a massive  $J^P = 2^+$  particle that has graviton-like couplings [25–28]. This model’s Lagrangian can be expressed as  $\mathcal{L}_{2^+} = \frac{c_V^G}{\Lambda} G^{\mu\nu} T_{\mu\nu}$ , where  $G^{\mu\nu}$  represents the  $J^P = 2^+$  particle,  $c_V^G$  is a coupling term,  $T_{\mu\nu}$  is the stress-energy tensor of the vector boson, and  $\Lambda$  is the effective Planck mass [8]. The mass of the non-SM Higgs-like particle  $X$  is set to 125 GeV, a value close to the mass measured by the LHC Collaborations [1, 2] and also consistent with measurements at the Tevatron [3]. We study the decay of  $X$  to  $b\bar{b}$  only. For our initial sample normalization we assume that the product of the cross section and the branching fraction,  $\sigma(VX) \times \mathcal{B}(X \rightarrow b\bar{b})$ , is equal to the SM value of 0.12 pb [29, 30]. We use the CTEQ6L1 PDF set for sample generation, and PYTHIA for parton showering and hadronization. The MC samples are processed by the full D0 detector simulation. To reproduce the effect of multiple  $p\bar{p}$  interactions in the same beam crossing, each simulated event is overlaid with an event from a sample of random beam crossings with the same instantaneous luminosity profile as the data. The events are then reconstructed with the same programs as the data.

The three contributing analyses are briefly described below. All analyses employ a  $b$ -tagging algorithm based on track impact parameters, secondary vertices, and event topology to select jets that are consistent with originating from a  $b$  quark [31, 32].

The  $ZH \rightarrow \ell\ell b\bar{b}$  analysis [15] selects events with two isolated charged leptons and at least two jets. A kinematic fit corrects the measured jet energies to their best fit values based on the constraints that the dilepton invariant mass should be consistent with the  $Z$  boson mass [33] and that the total transverse momentum of the leptons and jets should be consistent with zero. The event sample is further divided into orthogonal “single-tag” (ST) and “double-tag” (DT) channels according to the number of  $b$ -tagged jets. The SM Higgs boson search uses random forest (RF) [34] discriminants to provide distributions for the final statistical analysis. The first RF is designed to discriminate against  $t\bar{t}$  events and divides events into  $t\bar{t}$ -enriched and  $t\bar{t}$ -depleted ST and DT regions. In this study only events in the  $t\bar{t}$ -depleted ST and DT regions are considered. These regions contain  $\approx 94\%$  of the SM Higgs signal.

The  $WH \rightarrow \ell\nu b\bar{b}$  analysis [16] selects events with one charged lepton, significant imbalance in the transverse energy ( $\cancel{E}_T$ ), and two or three jets. This search is also sensitive to the  $ZH \rightarrow \ell\ell b\bar{b}$  process when one of the charged leptons is not identified. Using the outputs of the  $b$ -tagging algorithm for all selected jets, events are divided into four orthogonal  $b$ -tagging categories, “one-tight-tag” (1TT), “two-loose-tag” (2LT), “two-medium-



tag” (2MT), and “two-tight-tag” (2TT). Looser  $b$ -tagging categories correspond to higher efficiencies for true  $b$  quarks and higher fake rates. Outputs from boosted decision trees (BDTs) [34], trained separately for each jet multiplicity and tagging category, serve as the final discriminants in the SM Higgs boson search.

The  $ZH \rightarrow \nu\nu b\bar{b}$  analysis [17] selects events with large  $\cancel{E}_T$  and exactly two jets. This search is also sensitive to the  $WH$  process when the charged lepton from the  $W \rightarrow \ell\nu$  decay is not identified. A dedicated BDT is used to provide rejection of the large multijet background. Two orthogonal  $b$ -tagging channels, medium (MT), and tight (TT), are defined using the sum of the  $b$ -tagging discriminant outputs of the two selected jets. BDT classifiers, trained separately for the different  $b$ -tagging categories, provide the final discriminants in the SM Higgs boson search.

These three analyses are among the inputs to the D0 SM Higgs boson search [35], yielding an excess above the SM background expectation that is consistent with a SM Higgs boson signal. The best fit to data for the  $H \rightarrow b\bar{b}$  decay channel for the product of the signal cross section and branching fraction, expressed as a ratio to the SM prediction is  $\mu = 1.23^{+1.24}_{-1.17}$  for a mass of 125 GeV. When including data from both Tevatron experiments, the best fit to data yields  $\mu = 1.59^{+0.69}_{-0.72}$  [36].

Discrimination between the non-SM and the SM hypotheses is achieved by using mass information of the  $VX$  system. For the  $\ell\ell b\bar{b}$  final state we use the invariant mass of the two leptons and either the two highest  $b$ -tagged jets (DT) or the  $b$ -tagged jet and the highest  $p_T$  non-tagged jet (ST) as the final discriminating variable. For the final states that have neutrinos, the discriminating variable is the transverse mass of the  $VX$  system which is defined as  $M_T^2 = (E_T^V + E_T^X)^2 - (\vec{p}_T^V + \vec{p}_T^X)^2$  where the transverse momenta of the  $Z$  and  $W$  bosons are  $\vec{p}_T^Z = \vec{\cancel{E}}_T$  and  $\vec{p}_T^W = \vec{\cancel{E}}_T + \vec{p}_T^\ell$ . For the  $\ell\nu b\bar{b}$  final state the two jets can either be one  $b$ -tagged jet (1TT) and the highest  $p_T$  non-tagged jet, or the two  $b$ -tagged jets from any of the other three  $b$ -tagging categories: 2LT, 2MT, or 2TT. For the  $\nu\nu b\bar{b}$  final state the two jets are from either the medium (MT) or tight (TT)  $b$ -tagging channels.

To improve the discrimination between the non-SM signals and backgrounds in the  $\ell\ell b\bar{b}$  and  $\nu\nu b\bar{b}$  final states, we use the invariant mass of the dijet system,  $M_{jj}$ , to select two regions with different signal purities. Events with dijet masses in the range  $100 \leq M_{jj} \leq 150$  GeV ( $70 \leq M_{jj} < 150$  GeV) for  $\ell\ell b\bar{b}$  ( $\nu\nu b\bar{b}$ ) final states comprise the “high-purity” region (HP), while the remaining events are in the “low-purity region” (LP). For the  $\ell\nu b\bar{b}$  final state we use the final BDT output ( $\mathcal{D}$ ) of the SM Higgs boson search as described in Ref. [16]. Since events with  $\mathcal{D} \leq 0$  provide negligible sensitivity to SM or non-SM signals, we do not consider them further. We separate the remaining events into two categories with different signal purities. The LP category consists of events

with  $0 \leq \mathcal{D} \leq 0.5$ , and the HP category of events with  $\mathcal{D} > 0.5$ .

Figure 1 illustrates the discriminating variables for the three analysis channels in the high-purity categories for the most sensitive  $b$ -tagging selections. Distributions for additional subchannels can be found in Ref. [37].

We perform the statistical analysis using a modified frequentist approach [35, 38, 39]. We use a negative log-likelihood ratio (LLR) as the test statistic for two hypotheses: the null hypothesis,  $H_0$ , and the test hypothesis,  $H_1$ . This LLR is given by

$$\text{LLR} = -2 \ln \left( \frac{L_{H_1}}{L_{H_0}} \right), \quad (1)$$

where  $L_{H_x}$  is the joint likelihood for hypothesis  $x$  evaluated over the number of bins in the final discriminating variable distribution in each channel. To decrease the effect of systematic uncertainties on the sensitivity, we fit the signals and backgrounds by maximizing the likelihood functions by allowing the systematic effects to vary within Gaussian constraints. This fit is performed separately for both the  $H_0$  and  $H_1$  hypotheses for the data and each pseudo-experiment.

We define  $CL_s$  as

$$CL_s = \frac{CL_{H_1}}{CL_{H_0}} \quad (2)$$

where  $CL_{H_x}$  for a given hypothesis  $H_x$  is

$$CL_{H_x} = P_{H_x}(\text{LLR} \geq \text{LLR}^{\text{obs}}), \quad (3)$$

and  $\text{LLR}^{\text{obs}}$  is the LLR value observed in the data.  $P_{H_x}$  is defined as the probability that the LLR falls beyond  $\text{LLR}^{\text{obs}}$  for the distribution of LLR populated by the  $H_x$  model. For example, if  $CL_s \leq 0.05$  we exclude the  $H_1$  hypothesis in favor of the  $H_0$  hypothesis at  $\geq 95\%$  CL.

Systematic uncertainties affecting both shape and rate are considered. The systematic uncertainties for each individual analysis are described in Refs. [15–17]. A summary of the major contributions follows. The largest contribution for all analyses is from the uncertainties on the cross sections of the simulated  $V$ + heavy-flavor jets backgrounds which are 20%–30%. All other cross section uncertainties for simulated backgrounds are less than 10%. Since the multijet background is estimated from data, its uncertainty depends on the size of the data sample from which it is estimated, and ranges from 10% to 30%. All simulated samples for the  $WH \rightarrow \ell\nu b\bar{b}$  and  $ZH \rightarrow \nu\nu b\bar{b}$  analyses have an uncertainty of 6.1% from the integrated luminosity [40], whereas the simulated samples from the  $ZH \rightarrow \ell\ell b\bar{b}$  analysis have uncertainties ranging from 0.7%–7% arising from the fitted normalization to the data [15]. All analyses take into account uncertainties on the jet energy scale, resolution, and jet identification efficiency for a combined uncertainty of  $\approx 7\%$ . The uncertainty on the  $b$ -tagging

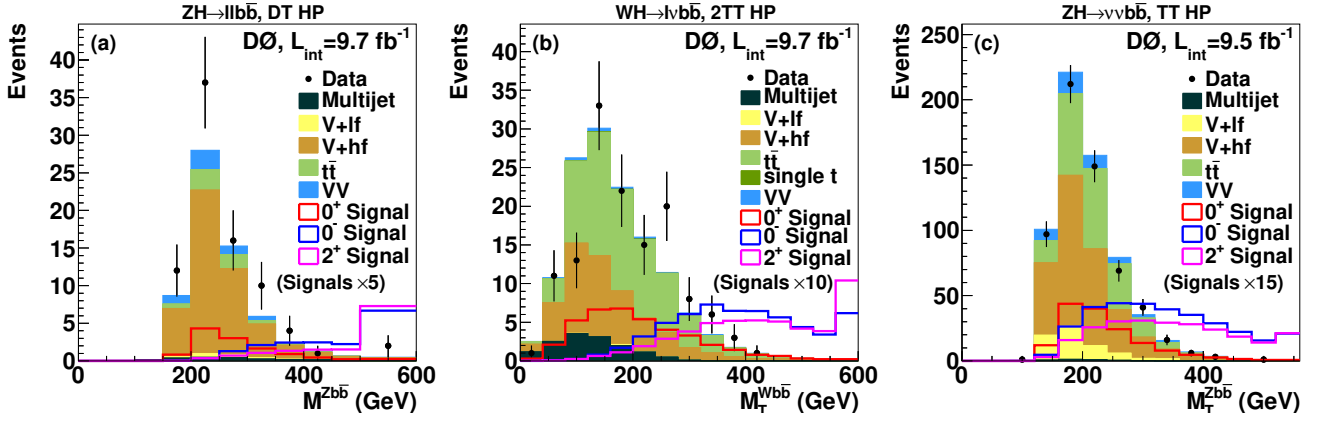


FIG. 1: (color online) (a) Invariant mass of the  $\ell\ell b\bar{b}$  system in the  $ZH \rightarrow \ell\ell b\bar{b}$  high-purity double-tag (DT HP) channel, (b) transverse mass of the  $\ell\nu b\bar{b}$  system in the  $WH \rightarrow \ell\nu b\bar{b}$  high-purity 2-tight-tag (2TT HP) channel, and (c) transverse mass of the  $\nu\nu b\bar{b}$  system in the  $ZH \rightarrow \nu\nu b\bar{b}$  high-purity tight-tag (TT HP) channel. The  $J^P = 0^-$  and  $J^P = 2^+$  samples are normalized to the product of the SM cross section and branching fraction multiplied by an additional factor for visibility. Heavy- and light-flavor quark jets are denoted by lf and hf, respectively. Overflow events are included in the highest mass bin. For all signals, a mass of 125 GeV for the  $H$  or  $X$  boson is assumed.

rate varies from 1%–10% depending on the number and quality of the tagged jets. The correlations between the three analyses are described in Ref. [35].

In this Letter, the  $H_0$  hypothesis always contains SM background processes and the SM Higgs boson normalized to  $\mu \times \sigma_{0^+}^{SM}$ . To test the non-SM cross section we assign the  $H_1$  hypothesis as the sum of the  $J^P = 0^-$  or  $J^P = 2^+$  signal plus SM background processes, with no contribution from the SM Higgs boson. We calculate the  $CL_s$  values using signal cross sections expressed as  $\mu \times \sigma_{0^+}^{SM}$  and evaluate the expected values for each of these quantities by replacing  $LLR^{\text{obs}}$  with  $LLR_{0^+}^{\text{exp}}$ , the median expectation for the  $J^P = 0^+$  hypothesis. Figure 2 illustrates the LLR distributions for the  $H_0$  and  $J^P = 2^+$   $H_1$  hypotheses, and the observed LLR value. We interpret  $1 - CL_s$  as the confidence level at which we exclude the non-SM hypothesis in favor of the SM prediction of  $J^P = 0^+$  for the given value of  $\mu$ . For  $\mu = 1.0$  we exclude the  $J^P = 0^-$  ( $J^P = 2^+$ ) hypothesis at the 97.6% (99.0%) CL. The expected exclusions are at the 99.86% and 99.94% CL.

Tables detailing the  $CL_{H_x}$  values for each individual analysis channel and the combination can be found in Ref. [37]. We also scan  $1 - CL_s$  over a range of SM and non-SM signal strengths. Figure 3 shows the expected and observed 95% CL exclusions as a function of the  $J^P = 0^-$  ( $J^P = 2^+$ ) and  $J^P = 0^+$  signal strengths, which may differ between the SM and non-SM signals. In the tests shown in Fig. 3 the signal in the  $H_1$  hypothesis is the  $J^P = 0^-$  ( $J^P = 2^+$ ) signal normalized to  $\mu_{0^-}$  ( $\mu_{2^+}$ )  $\times \sigma_{0^+}^{SM}$ , and the signal in the  $H_0$  hypothesis is the  $J^P = 0^+$  signal normalized to  $\mu_{0^+} \times \sigma_{0^+}^{SM}$ .

We also consider the possibility of a combination of  $J^P$  signals in our data (e.g.,  $J^P = 0^+$  and  $J^P = 0^-$ ).

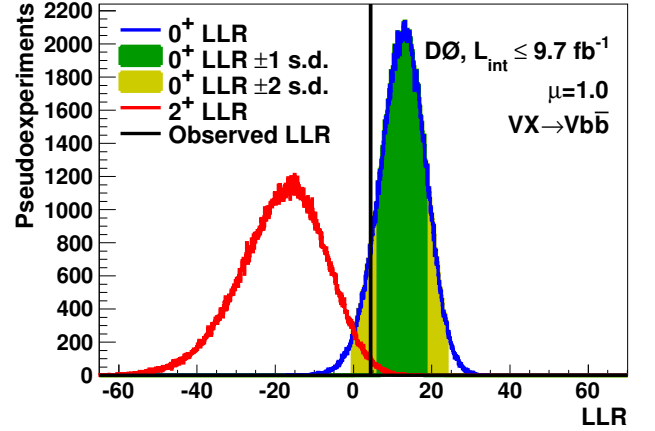


FIG. 2: (color online) LLR distributions comparing the  $J^P = 0^+$  and the  $J^P = 2^+$  hypotheses for the combination. The  $J^P = 0^+$  and  $J^P = 2^+$  samples are normalized to the product of the SM cross section and branching fraction multiplied by  $\mu = 1.0$ . The vertical solid line represents the observed LLR value, while the dark and light shaded areas represent the 1 and 2 standard deviations (s.d.) on the expectation from the null hypothesis  $H_0$ , respectively.

These tests provide constraints on a number of theoretical models such as those containing pseudoscalar bosons in addition to a SM-like Higgs boson. For these studies we fix the sum of the two cross sections to a specific value of  $\mu \times \sigma_{0^+}^{SM}$  and vary the fractions  $f_{0^-} = \sigma_{0^-} / (\sigma_{0^+} + \sigma_{0^-})$  or  $f_{2^+} = \sigma_{2^+} / (\sigma_{0^+} + \sigma_{2^+})$  of non-SM signal and calculate the same  $CL_s$  values as above as a function of  $f_{0^-}$  or  $f_{2^+}$ . To study  $f_{0^-}$ , we now modify  $H_1$  to be the sum of the background, the  $J^P = 0^-$  signal normalized to  $\mu \times \sigma_{0^+}^{SM} \times f_{0^-}$ , and the  $J^P = 0^+$  signal normalized to  $\mu \times \sigma_{0^+}^{SM} \times (1 - f_{0^-})$ .  $H_0$  remains as previously defined.

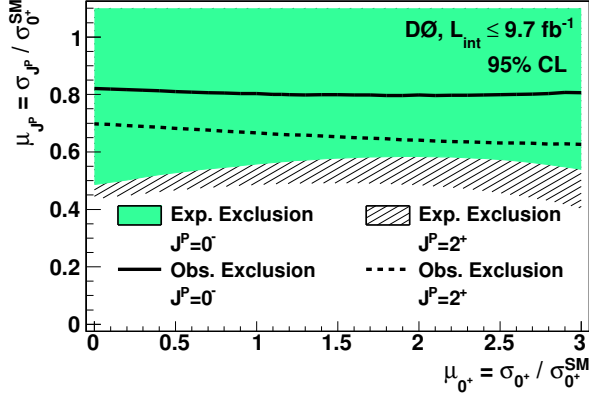


FIG. 3: (color online) The expected exclusion region (shaded area) and observed exclusion (solid line) as functions of the  $J^P = 0^-$  and  $J^P = 0^+$  signal strengths. The expected exclusion region (hatched area) and observed exclusion (dashed line) as functions of the  $J^P = 2^+$  and  $J^P = 0^+$  signal strengths.

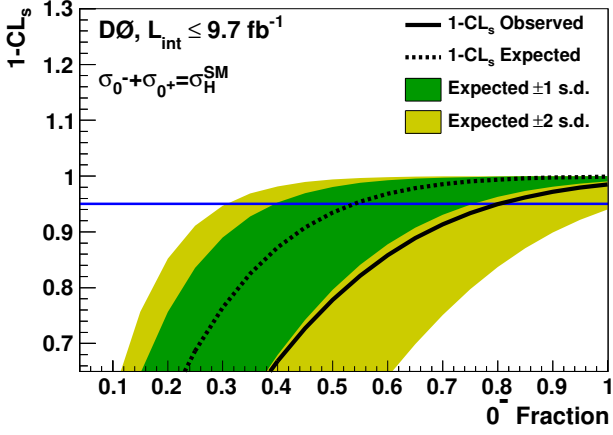


FIG. 4: (color online)  $1 - CL_s$  as a function of the  $J^P = 0^-$  signal fraction. The horizontal blue line corresponds to the 95% CL exclusion for  $\mu = 1.0$ . The dark and light shaded regions represent the 1 and 2 standard deviations (s.d.) fluctuations for the  $J^P = 0^+$  hypothesis.

We follow an identical prescription for  $J^P = 2^+$ . Figure 4 presents the value  $1 - CL_s$  as a function of the  $J^P = 0^-$  signal fraction  $f_{0^-}$  for the case of  $\mu = 1.0$ , and the corresponding figure for the  $J^P = 2^+$  hypothesis is available in Ref. [37]. For  $\mu = 1.0$  we exclude a  $J^P = 0^-$  ( $J^P = 2^+$ ) signal fraction  $f_{0^-} > 0.80$  ( $f_{2^+} > 0.67$ ) at the 95% CL. The expected exclusions are  $f_{0^-} > 0.54$  ( $f_{2^+} > 0.47$ ).

In summary, we have performed a study of possible spin and parity assignments for the Higgs boson produced in association with a  $W$  or  $Z$  boson and decaying into  $b\bar{b}$  pairs. We use the published analyses of the  $WH \rightarrow \ell\nu b\bar{b}$ ,  $ZH \rightarrow \ell\ell b\bar{b}$ , and  $ZH \rightarrow \nu\nu b\bar{b}$  final states with no modifications to the event selections. Sensitivity to non-SM  $J^P$  assignments is enhanced via the separation

of samples into high- and low-purity categories wherein the total mass or total transverse mass of the  $VX$  system provides powerful discrimination. Our data strongly prefer a  $J^P = 0^+$  value, in agreement with the SM prediction. These results are summarized in Table I. We

$J^P$	$1 - CL_s$ (s.d.)		$f_{J^P}$	
$\mu = 1.0$	Exp.	Obs.	Exp.	Obs.
$0^-$	0.9986 (3.00)	0.976 (1.98)	$>0.54$	$>0.80$
$2^+$	0.9994 (3.22)	0.990 (2.34)	$>0.47$	$>0.67$
$\mu = 1.23$				
$0^-$	0.9998 (3.60)	0.995 (2.56)	$>0.45$	$>0.67$
$2^+$	0.9999 (3.86)	0.998 (2.91)	$>0.40$	$>0.56$

TABLE I: Expected and observed  $1 - CL_s$  values (converted to s.d. in parentheses) and signal fractions for  $\mu = 1.0$  and  $\mu = 1.23$  excluded at the 95% CL.

are able to reject the  $J^P = 0^-$  and  $J^P = 2^+$  hypotheses and set limits on the non-SM signal fraction in our data. This is the first exclusion in a fermionic decay channel of the  $J^P = 0^-$  and  $J^P = 2^+$  hypotheses for the spin and parity of the Higgs boson.

We thank the staffs at Fermilab and collaborating institutions, and acknowledge support from the DOE and NSF (USA); CEA and CNRS/IN2P3 (France); MON, NRC KI and RFBR (Russia); CNPq, FAPERJ, FAPESP and FUNDUNESP (Brazil); DAE and DST (India); Colciencias (Colombia); CONACyT (Mexico); NRF (Korea); FOM (The Netherlands); STFC and the Royal Society (United Kingdom); MSMT and GACR (Czech Republic); BMBF and DFG (Germany); SFI (Ireland); The Swedish Research Council (Sweden); and CAS and CNSF (China).

- 
- [1] G. Aad *et al.* [ATLAS Collaboration], Phys. Lett. B **716**, 1 (2012).
  - [2] S. Chatrchyan *et al.* [CMS Collaboration], Phys. Lett. B **716**, 30 (2012).
  - [3] T. Aaltonen *et al.* [CDF and D0 Collaborations], Phys. Rev. Lett. **109**, 071804 (2012).
  - [4] L. Landau, Dokl. Akad. Nauk Ser. Fiz. **60**, 207 (1948).
  - [5] C. N. Yang, Phys. Rev. **77**, 242 (1950).
  - [6] T. D. Lee, Phys. Rev. D **8**, 1226 (1973).
  - [7] E. Cerveró and J.-M. Gérard, Phys. Lett. B **712**, 255 (2012).
  - [8] R. Fok, C. Guimaraes, R. Lewis, and V. Sanz, J. High Energy Phys. **12**, 062 (2012).
  - [9] G. Aad *et al.* [ATLAS Collaboration], Phys. Lett. B **726**, 120 (2013).
  - [10] S. Chatrchyan *et al.* [CMS Collaboration], Phys. Rev. Lett. **110**, 081803 (2013).
  - [11] S. Chatrchyan *et al.* [CMS Collaboration], J. High Energy Phys. **01**, 096 (2014).

- [12] J. Ellis, D. S. Hwang, V. Sanz, and T. You, J. High Energy Phys. **12**, 134 (2012).
- [13] J. Ellis, V. Sanz, and T. You, Eur. Phys. J. C **73**, 1 (2013).
- [14] D. Miller, S. Choi, B. Eberle, M. Mühlleitner, and P. Zerwas, Phys. Lett. B **505**, 149 (2001).
- [15] V. M. Abazov *et al.* [D0 Collaboration], Phys. Rev. D **88**, 052010 (2013).
- [16] V. M. Abazov *et al.* [D0 Collaboration], Phys. Rev. D **88**, 052008 (2013).
- [17] V. M. Abazov *et al.* [D0 Collaboration], Phys. Lett. B **716**, 285 (2012).
- [18] V. M. Abazov *et al.* [D0 Collaboration], Nucl. Instrum. Methods Phys. Res. A **565**, 463 (2006).
- [19] M. Abolins *et al.*, Nucl. Instrum. Methods Phys. Res. A **584**, 75 (2008).
- [20] R. Angstadt *et al.*, Nucl. Instrum. Methods Phys. Res. A **622**, 298 (2010).
- [21] M. L. Mangano, M. Moretti, F. Piccinini, R. Pittau, and A. D. Polosa, J. High Energy Phys. **07**, 001 (2003).
- [22] E. E. Boos, V. E. Bunichev, L. V. Dudko, V. I. Savrin, and V. V. Sherstnev, Phys. Atom. Nucl. **69**, 1317 (2006).
- [23] T. Sjöstrand, S. Mrenna, and P. Z. Skands, J. High Energy Phys. **05**, 026 (2006).
- [24] J. Alwall, M. Herquet, F. Maltoni, O. Mattelaer, and T. Stelzer, J. High Energy Phys. **06**, 128 (2011). We use version 1.4.8.4.
- [25] L. Randall and R. Sundrum, Phys. Rev. Lett. **83**, 3370 (1999).
- [26] L. Randall and R. Sundrum, Phys. Rev. Lett. **83**, 4690 (1999).
- [27] K. Hagiwara, J. Kanzaki, Q. Li, and K. Mawatari, Eur. Phys. J. C **56**, 435 (2008).
- [28] P. Aquino, K. Hagiwara, Q. Li, and F. Maltoni, J. High Energy Phys. **11**, 1 (2011).
- [29] J. Baglio and A. Djouadi, J. High Energy Phys. **10**, 064 (2010).
- [30] O. Brein, R. V. Harlander, M. Wiesemann, and T. Zirke, Eur. Phys. J. C **72**, 1 (2012).
- [31] V. M. Abazov *et al.* [D0 Collaboration], Nucl. Instrum. Methods Phys. Res. A **763**, 290 (2014).
- [32] V. M. Abazov *et al.* [D0 Collaboration], Nucl. Instrum. Methods Phys. Res. A **620**, 490 (2010).
- [33] J. Beringer *et al.*, Particle Data Group, Phys. Rev. D **86**, 010001 (2012), and 2013 partial update for the 2014 edition.
- [34] A. Hoecker *et al.*, PoS **ACAT**, 040 (2007). We use version 4.1.0.
- [35] V. M. Abazov *et al.* [D0 Collaboration], Phys. Rev. D **88**, 052011 (2013).
- [36] T. Aaltonen *et al.* [CDF and D0 Collaborations], Phys. Rev. D **88**, 052014 (2013).
- [37] See EPAPS Document No. xxxx for additional figures.
- [38] A. L. Read, J. Phys. G **28**, 2693 (2002).
- [39] W. Fisher, FERMILAB-TM-2386-E (2007).
- [40] T. Andeen *et al.*, FERMILAB-TM-2365 (2007).

---

## SUPPLEMENTAL MATERIAL

In this document we provide supplemental information on the constraints on the spin and parity for the Higgs boson in the  $VH \rightarrow Vb\bar{b}$  final states in up to  $9.7 \text{ fb}^{-1}$  of  $p\bar{p}$  collisions at  $\sqrt{s} = 1.96 \text{ TeV}$  collected with the D0 detector at the Fermilab Tevatron Collider. We denote a non-SM Higgs boson as  $X$ .

**Figure 5:** Dijet mass distributions for the  $\nu\nu b\bar{b}$  and  $\ell\ell b\bar{b}$  analyses and the BDT output distribution for the  $\ell\nu b\bar{b}$  analysis.

**Figures 6–9:** Additional  $VX$  invariant and transverse mass distributions for individual analyses.

**Figures 10 and 11:** LLR distributions for the individual analyses and their combination.

**Tables II and III:** Tables of  $CL_{H_x}$  and  $1 - CL_s$  values for the individual analyses and their combination for  $\mu = 1.0$  and  $\mu = 1.23$ .

**Figure 12:**  $1 - CL_s$  as a function of the  $J^P = 2^+$  signal fraction,  $f_{2^+}$ , for all analyses combined.

**Figure 13:** The expected and observed 95% CL exclusion as functions of the  $J^P = 0^-$  ( $J^P = 2^+$ ) signal fraction,  $f_{0^-}$  ( $f_{2^+}$ ), and the total signal strength.



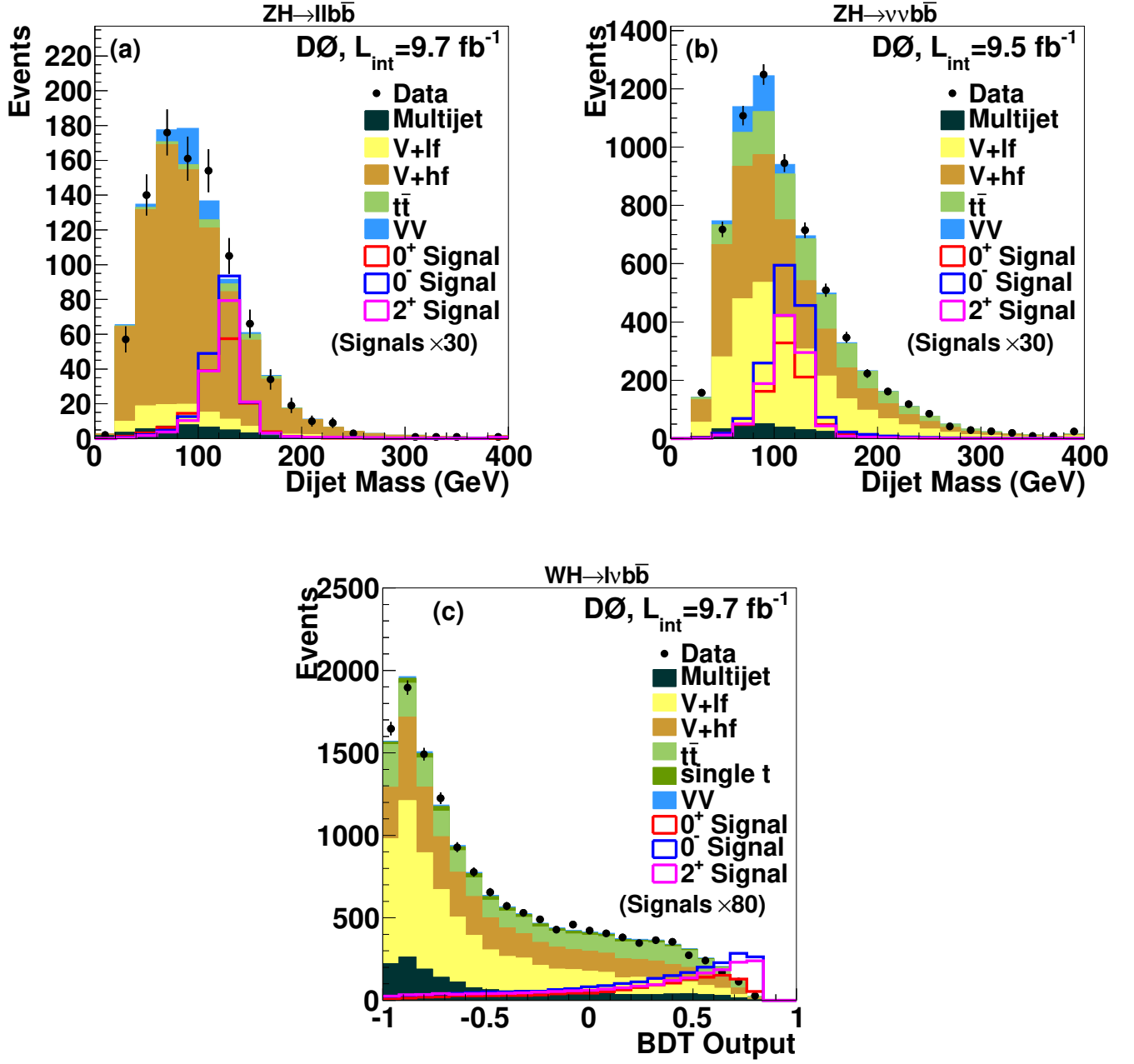


FIG. 5: Invariant mass of the dijet system for (a) the  $ZH \rightarrow \ell\ell b\bar{b}$  analysis, and (b) the  $ZH \rightarrow \nu\nu b\bar{b}$  analysis, and the BDT output for (c) the  $WH \rightarrow \ell\nu b\bar{b}$  analysis. The  $J^P = 2^+$  and  $J^P = 0^-$  samples are normalized to the product of the SM cross section and branching fraction multiplied by an additional factor for visibility. Heavy- and light-flavor quark jets are denoted by lf and hf, respectively. Overflow events are included in the highest bin. For all signals, a mass of 125 GeV for the  $H$  or  $X$  boson is assumed.

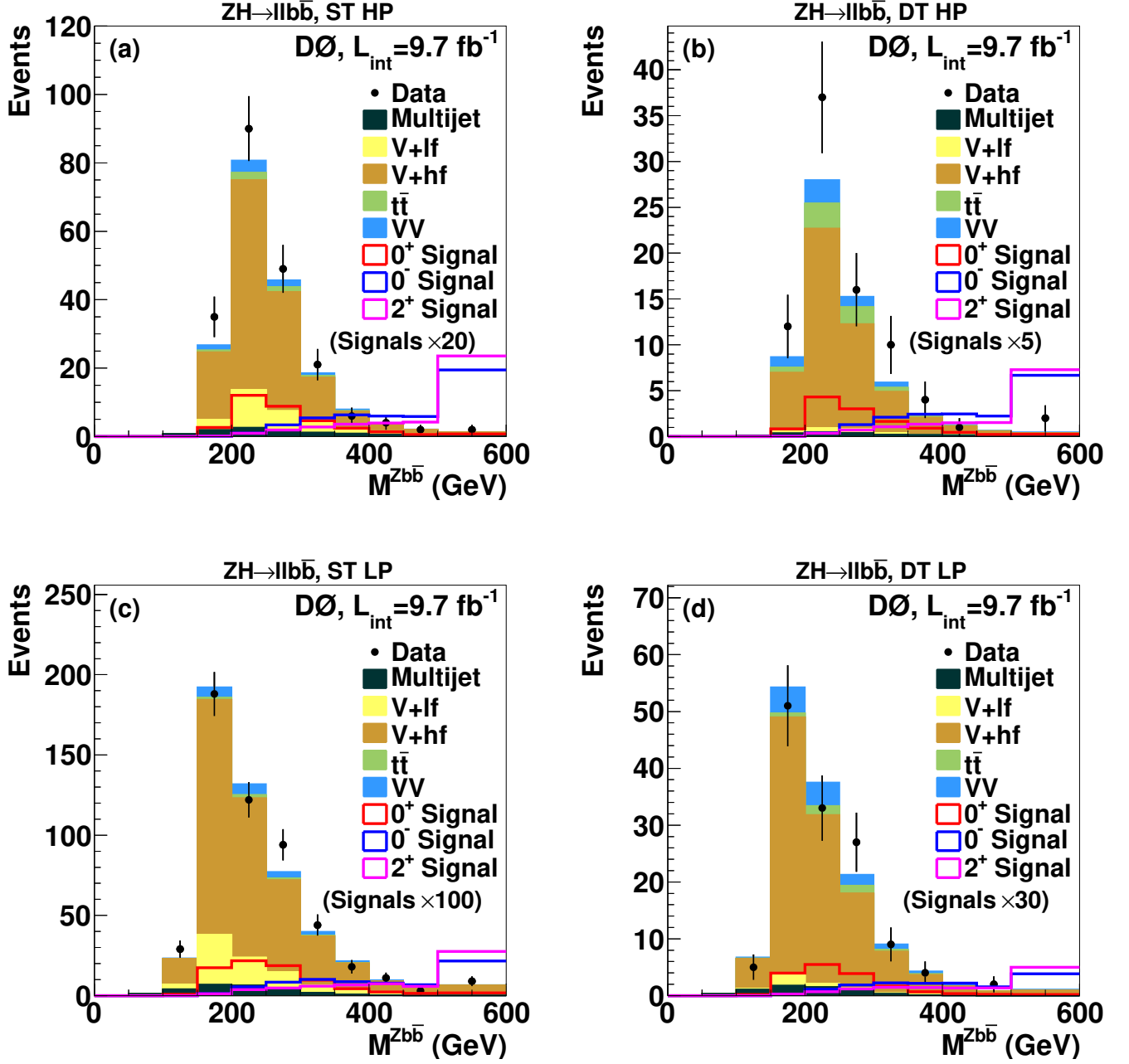


FIG. 6: Invariant mass of the  $\ell\ell b\bar{b}$  system in the  $ZH \rightarrow \ell\ell b\bar{b}$  analysis for events in the (a) single-tag high-purity (ST HP), (b) double-tag high-purity (DT HP), (c) single-tag low-purity (ST LP), and (d) double-tag low-purity (DT LP) channels. The  $J^P = 2^+$  and  $J^P = 0^-$  samples are normalized to the product of the SM cross section and branching fraction multiplied by an additional factor for visibility. Heavy- and light-flavor quark jets are denoted by lf and hf, respectively. Overflow events are included in the last bin. For all signals, a mass of 125 GeV for the  $H$  or  $X$  boson is assumed.

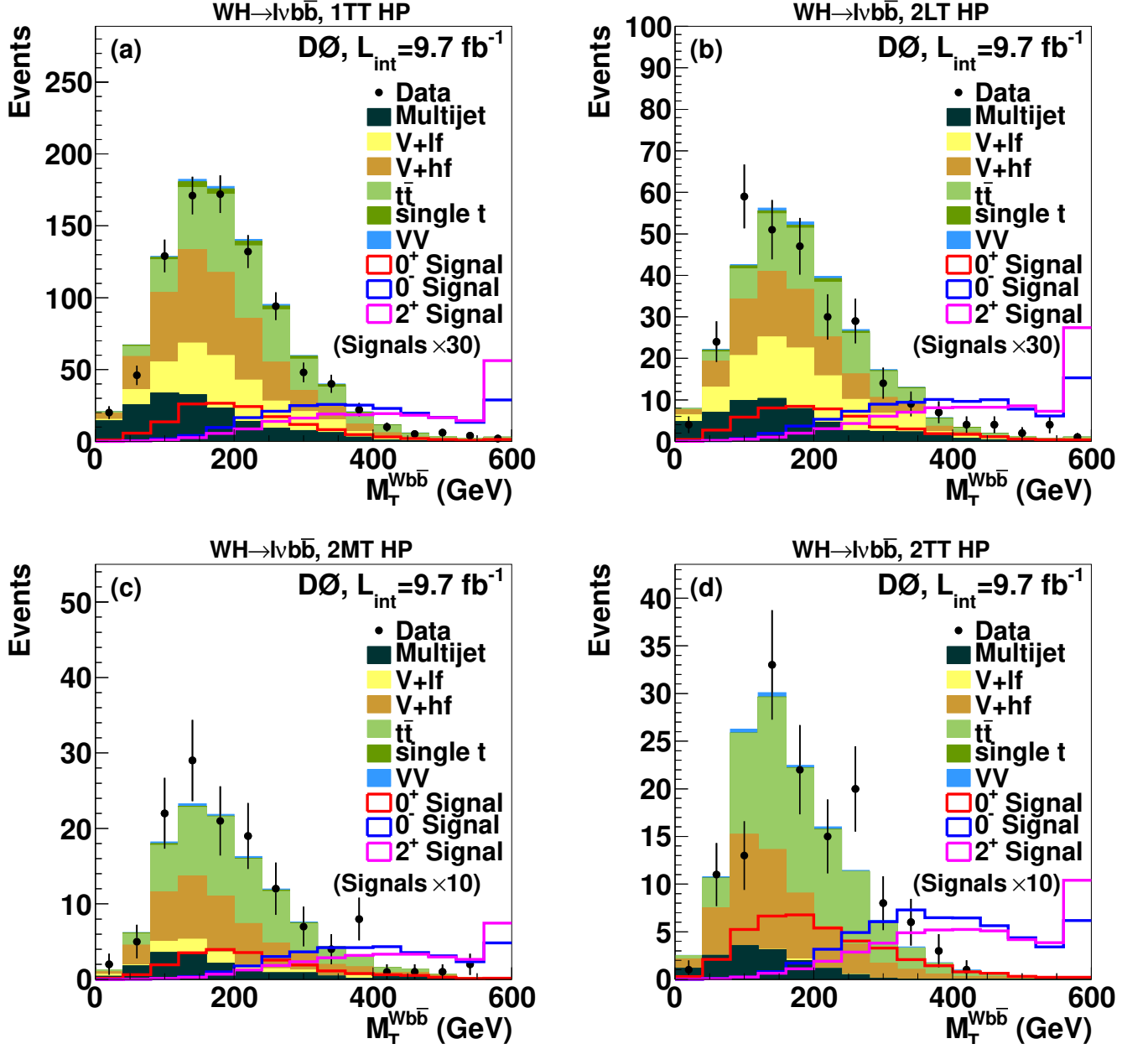


FIG. 7: Transverse mass of the  $\ell\nu b\bar{b}$  system in the  $WH \rightarrow \ell\nu b\bar{b}$  analysis in the high-purity (HP) region for (a) 1 tight-tag (1TT), (b) 2 loose-tags (2LT), (c) 2 medium-tags (2MT), and (d) 2 tight-tags (2TT) channels. The  $J^P = 2^+$  and  $J^P = 0^-$  samples are normalized to the product of the SM cross section and branching fraction multiplied by an additional factor for visibility. Heavy- and light-flavor quark jets are denoted by lf and hf, respectively. Overflow events are included in the last bin. For all signals, a mass of 125 GeV for the  $H$  or  $X$  boson is assumed.

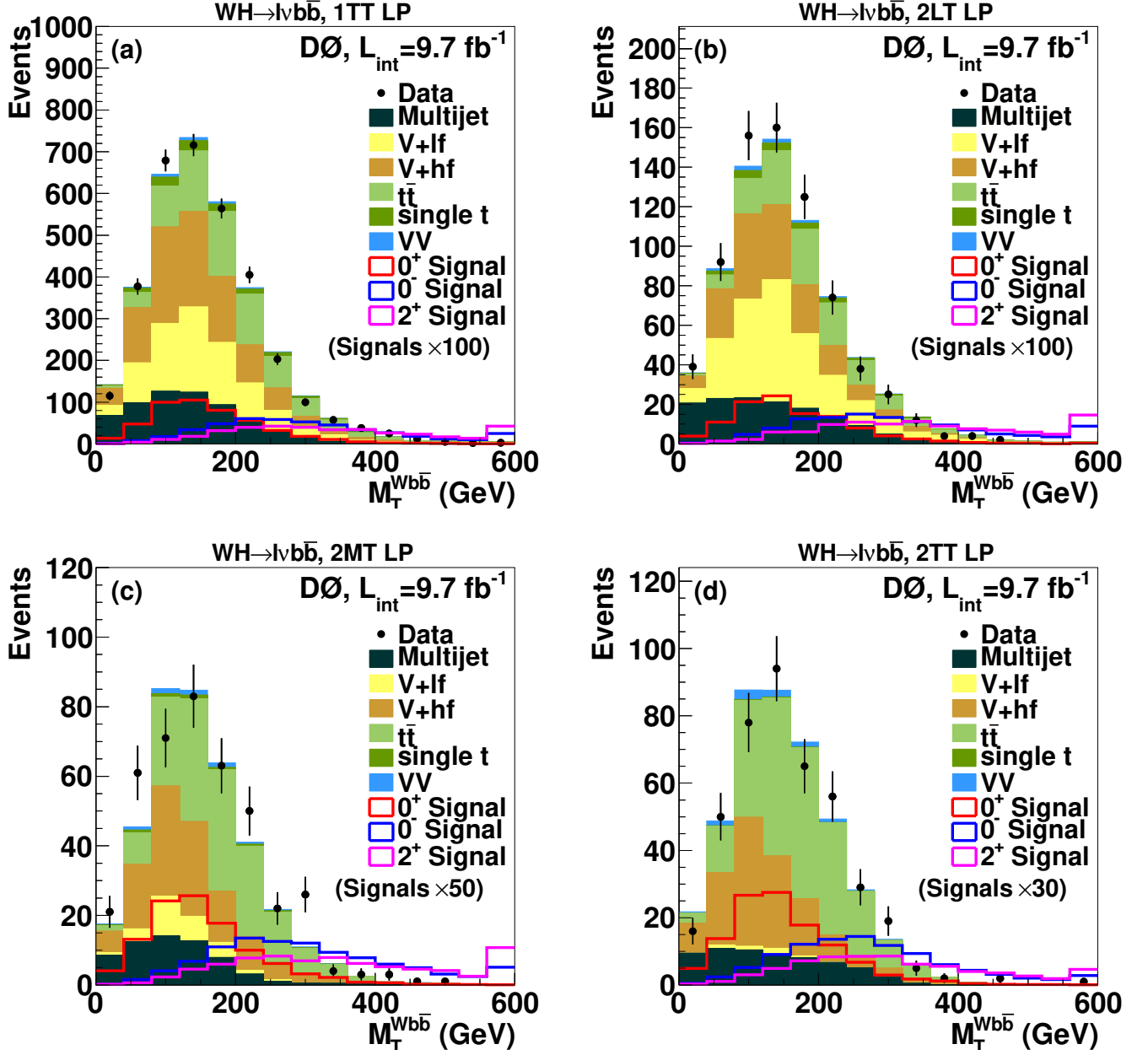


FIG. 8: Transverse mass of the  $l\nu b\bar{b}$  system in the  $WH \rightarrow l\nu b\bar{b}$  analysis in the low purity (LP) region for (a) 1-tight-tag (1TT), (b) 2-loose-tags (2LT), (c) 2-medium-tags (2MT), and (d) 2-tight-tags (2TT) channels. The  $J^P = 2^+$  and  $J^P = 0^-$  samples are normalized to the product of the SM cross section and branching fraction multiplied by an additional factor for visibility. Heavy- and light-flavor quark jets are denoted by lf and hf, respectively. Overflow events are included in the last bin. For all signals, a mass of 125 GeV for the  $H$  or  $X$  boson is assumed.



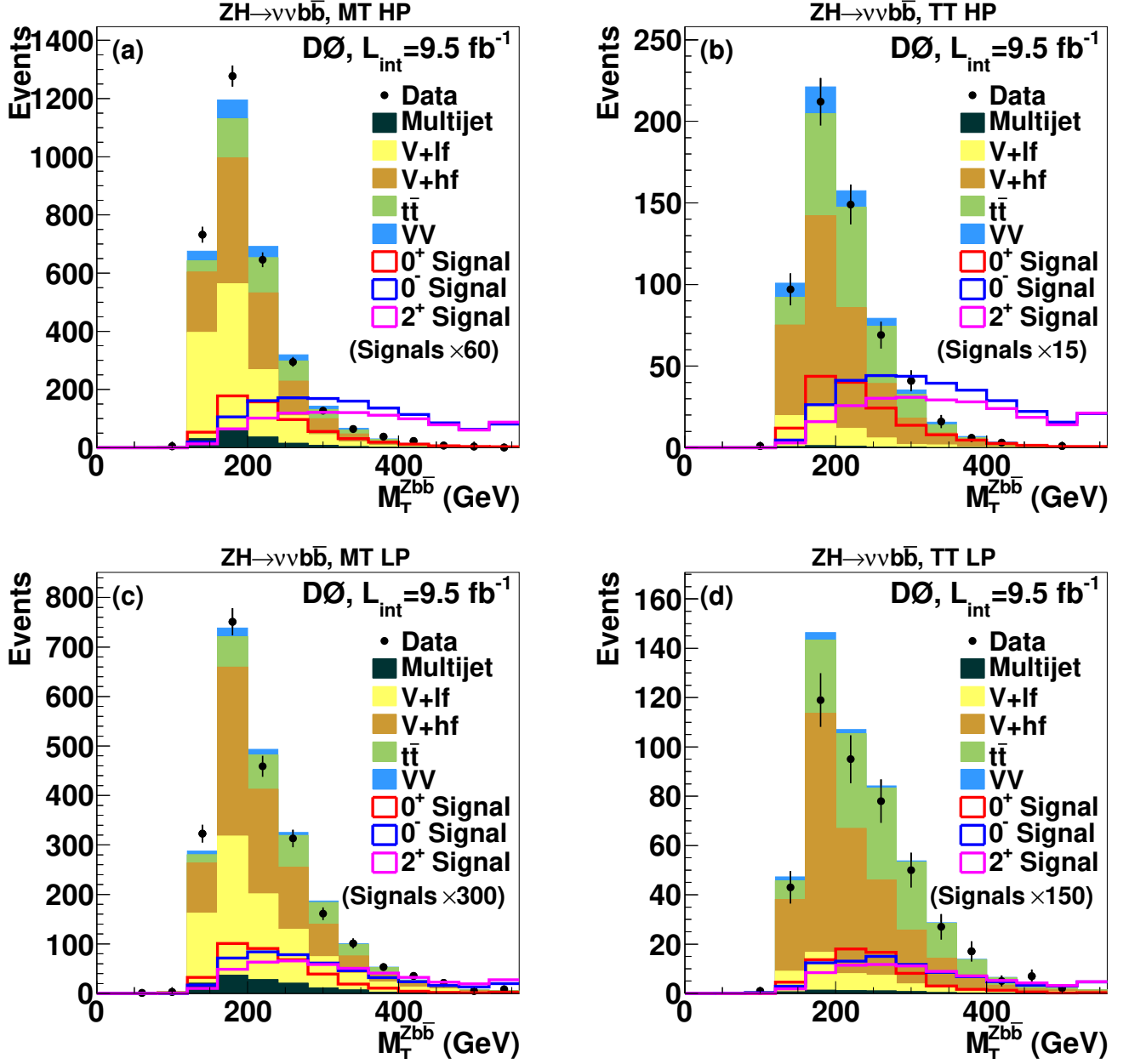


FIG. 9: Transverse mass of the  $\nu\nu b\bar{b}$  system in the  $ZH \rightarrow \nu\nu b\bar{b}$  analysis for events in the (a) medium-tag high-purity (MT HP), (b) tight-tag high-purity (TT HP), (c) medium-tag low-purity (MT LP), and (d) tight-tag low-purity (TT LP) channels. The  $J^P = 2^+$  and  $J^P = 0^-$  samples are normalized to the product of the SM cross section and branching fraction multiplied by an additional factor for visibility. Heavy- and light-flavor quark jets are denoted by lf and hf, respectively. Overflow events are included in the last bin. For all signals, a mass of 125 GeV for the  $H$  or  $X$  boson is assumed.

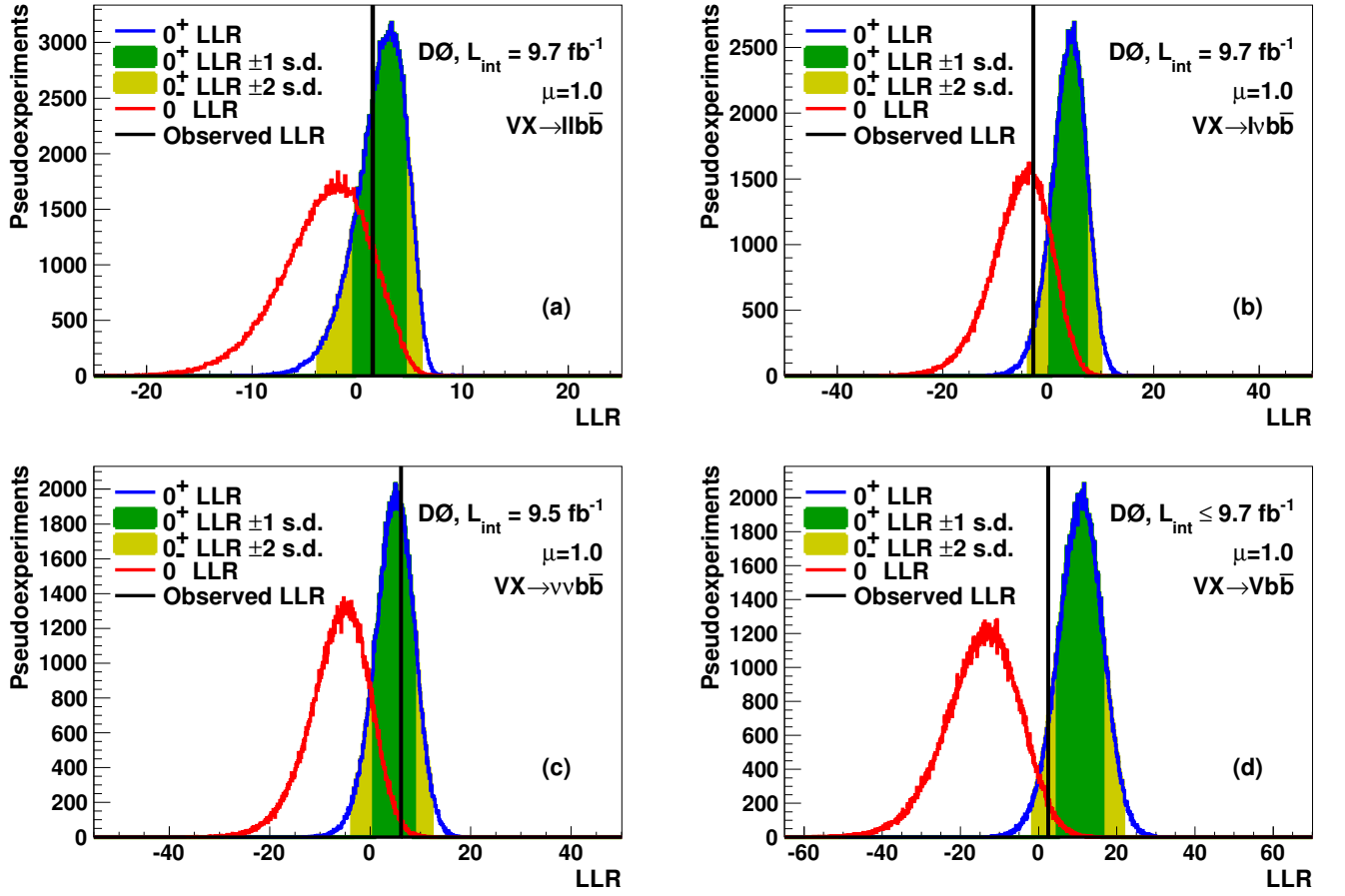


FIG. 10: LLR distributions comparing the  $J^P = 0^+$  and the  $J^P = 0^-$  hypotheses for the (a)  $ZH \rightarrow \ell\ell b\bar{b}$  analysis, (b)  $WH \rightarrow \ell\nu b\bar{b}$  analysis, (c)  $ZH \rightarrow \nu\nu b\bar{b}$  analysis, and (d) their combination. The  $J^P = 0^+$  and  $J^P = 0^-$  samples are normalized to the product of the SM cross section and branching fraction multiplied by  $\mu = 1.0$ . The vertical solid line represents the observed LLR value, while the dark and light shaded areas represent 1 s.d. and 2 s.d. on the expectation from the null hypothesis  $H_0$ , respectively. Here  $H_0$  is the SM  $J^P = 0^+$  signal plus backgrounds. For all signals, a mass of 125 GeV for the  $H$  or  $X$  boson is assumed.

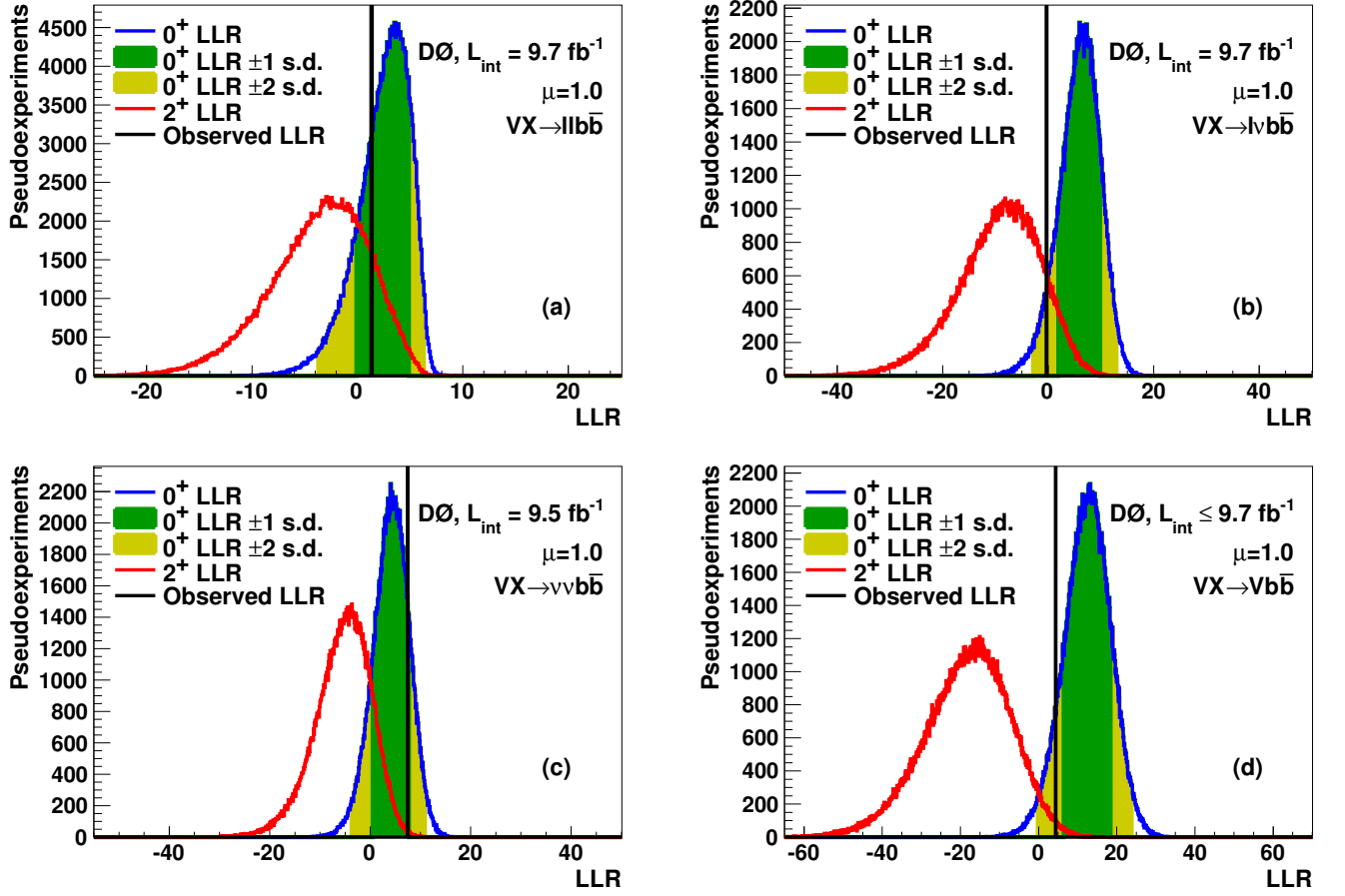


FIG. 11: LLR distributions comparing the  $J^P = 0^+$  and the  $J^P = 2^+$  hypotheses for the (a)  $ZH \rightarrow \ell\ell b\bar{b}$  analysis, (b)  $WH \rightarrow \ell\nu b\bar{b}$  analysis, (c)  $ZH \rightarrow \nu\nu b\bar{b}$  analysis, and (d) their combination. The  $J^P = 0^+$  and  $J^P = 2^+$  samples are normalized to the product of the SM cross section and branching fraction multiplied by  $\mu = 1.0$ . The vertical solid line represents the observed LLR value, while the dark and light shaded areas represent 1 s.d. and 2 s.d. on the expectation from the null hypothesis  $H_0$ , respectively. Here  $H_0$  is the SM  $J^P = 0^+$  signal plus backgrounds. For all signals, a mass of 125 GeV for the  $H$  or  $X$  boson is assumed.

Analysis	$ZH \rightarrow \ell\ell b\bar{b}$	$WH \rightarrow \ell\nu b\bar{b}$	$ZH \rightarrow \nu\nu b\bar{b}$	Combined
	$J^P = 0^-$ vs. $J^P = 0^+$			
$CL_{0-}$ Expected	0.075	0.030	0.016	0.0007
$CL_{0-}$ Observed	0.126	0.351	0.007	0.022
$CL_{0+}$ Expected	0.500	0.500	0.500	0.500
$CL_{0+}$ Observed	0.646	0.965	0.367	0.918
$1 - CL_s$ Expected	0.850 (1.04 s.d.)	0.941 (1.56 s.d.)	0.969 (1.87 s.d.)	0.9986 (3.00 s.d.)
$1 - CL_s$ Observed	0.805 (0.86 s.d.)	0.637 (0.35 s.d.)	0.981 (2.07 s.d.)	0.976 (1.98 s.d.)
	$J^P = 2^+$ vs. $J^P = 0^+$			
$CL_{2+}$ Expected	0.064	0.009	0.023	0.0003
$CL_{2+}$ Observed	0.134	0.114	0.002	0.009
$CL_{0+}$ Expected	0.500	0.500	0.500	0.500
$CL_{0+}$ Observed	0.702	0.932	0.173	0.906
$1 - CL_s$ Expected	0.872 (1.14 s.d.)	0.982 (2.09 s.d.)	0.953 (1.68 s.d.)	0.9994 (3.22 s.d.)
$1 - CL_s$ Observed	0.810 (0.88 s.d.)	0.878 (1.16 s.d.)	0.987 (2.23 s.d.)	0.990 (2.34 s.d.)

TABLE II: Expected and observed  $CL_{H_x}$  and  $1 - CL_s$  values for  $J^P = 0^-$  and  $J^P = 2^+$   $VX$  associated production, assuming signal cross sections equal to the 125 GeV SM Higgs production cross section multiplied by  $\mu = 1.0$ . The null hypothesis is taken to be the sum of the SM Higgs boson signal and background production.



Analysis	$ZH \rightarrow \ell\ell b\bar{b}$	$WH \rightarrow \ell\nu b\bar{b}$	$ZH \rightarrow \nu\nu b\bar{b}$	Combined
	$J^P = 0^-$ vs. $J^P = 0^+$			
$CL_{0-}$ Expected	0.046	0.012	0.005	<0.0001
$CL_{0-}$ Observed	0.072	0.245	0.0006	0.005
$CL_{0+}$ Expected	0.500	0.500	0.500	0.500
$CL_{0+}$ Observed	0.615	0.971	0.215	0.922
$1 - CL_s$ Expected	0.908 (1.33 s.d.)	0.975 (1.96 s.d.)	0.989 (2.31 s.d.)	0.9998 (3.60 s.d.)
$1 - CL_s$ Observed	0.883 (1.19 s.d.)	0.747 (0.67 s.d.)	0.997 (2.78 s.d.)	0.995 (2.56 s.d.)
	$J^P = 2^+$ vs. $J^P = 0^+$			
$CL_{2+}$ Expected	0.037	0.003	0.009	<0.0001
$CL_{2+}$ Observed	0.078	0.056	0.003	0.002
$CL_{0+}$ Expected	0.500	0.500	0.500	0.500
$CL_{0+}$ Observed	0.679	0.937	0.363	0.911
$1 - CL_s$ Expected	0.925 (1.44 s.d.)	0.995 (2.56 s.d.)	0.983 (2.11 s.d.)	0.9999 (3.86 s.d.)
$1 - CL_s$ Observed	0.885 (1.20 s.d.)	0.941 (1.56 s.d.)	0.991 (2.35 s.d.)	0.998 (2.91 s.d.)

TABLE III: Expected and observed  $CL_{H_x}$  and  $1 - CL_s$  values for  $J^P = 0^-$  and  $J^P = 2^+$   $VX$  associated production, assuming signal cross sections equal to the 125 GeV SM Higgs production cross section multiplied by  $\mu = 1.23$ . The null hypothesis is taken to be the sum of the SM Higgs boson signal and background production.

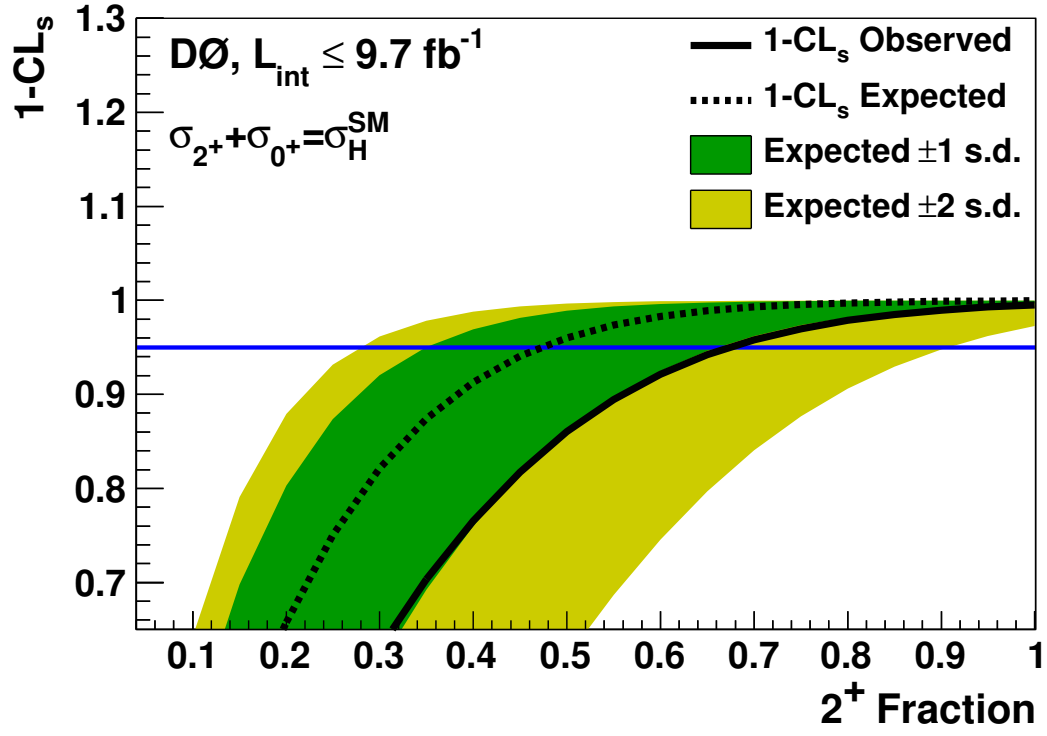


FIG. 12: (color online)  $1 - CL_s$  as a function of the  $J^P = 2^+$  signal fraction  $f_{2^+}$  for  $\mu = 1.0$  for all analyses combined. The horizontal solid line corresponds to the 95% CL exclusion. The dark and light shaded regions represent the expected 1 and 2 s.d. fluctuations of the  $J^P = 0^+$  hypothesis.

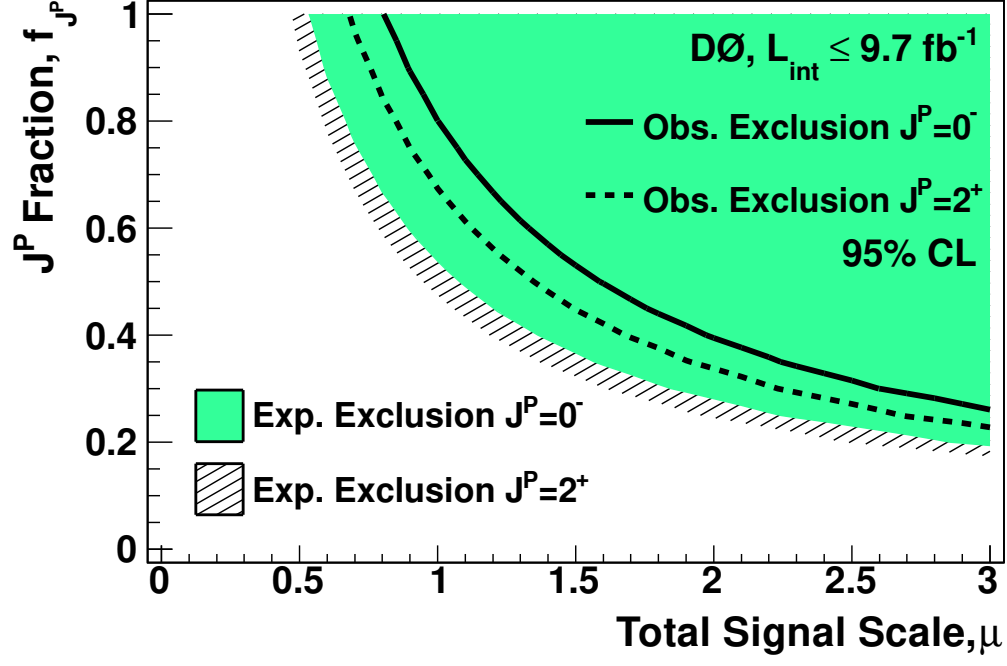


FIG. 13: (color online) The expected 95% CL exclusion (shaded area) and observed 95% CL exclusion (solid line) as functions of the  $J^P = 0^-$  signal fraction  $f_{0^-}$  and the total signal strength in units of the SM Higgs cross section multiplied by the branching ratio. As functions of the  $J^P = 2^+$  signal fraction  $f_{2^+}$  and the total signal strength, the expected and observed exclusions are shown as the hatched area and dashed line, respectively.